MRS Advances (2023) 8:602–606
https://doi.org/10.1557/s43580-023-00576-4

ORIGINAL PAPER

Investigation of network microstructure of TiB/Ti6Al4V-ELI composite manufactured with laser metal deposition

Paul M. Lekoadi[1,3] · Monnamme Tlotleng[1,2] · Charles W. Siyasiya[3] · Bathusile N. Masina[1,2]

Received: 23 January 2023 / Accepted: 19 April 2023 / Published online: 12 May 2023

Abstract

This work presents the microstructural investigation of an in situ synthesized TiB/Ti6Al4V-ELI composite that was manufactured with additive manufacturing (AM) technique known as laser metal deposition (LMD). A single-track sample was manufactured by adding TiB_2 to Ti6Al4V-ELI at mass deposition volume of 5% and characterized for microstructure and hardness. It was found that in situ reaction promoted the formation of quasi-continuous network microstructure of TiB whiskers with a needle-like morphology, in a martensitic α′ matrix. Furthermore, the manufactured TiB/Ti6Al4V-ELI presented two different grain growth morphologies, with smaller and large TiB network grains observed at the top and bottom of the sample, respectively, due to heat travelling direction. A high hardness of 513 HV was observed at the top of the sample, which was reduced to 483 HV at the bottom, promoted by grain growth.

Introduction

Titanium alloys including Ti6Al4V are widely used in the aerospace, aeronautical, and biomedical industries, due to their desirable properties of low density, high specific strength, biocompatibility, and excellent corrosion resistance [1, 2]. Ti6Al4V has a dual-phase microstructure, which consists of hexagonal closed packed (hcp) α phase and body-centred cubic (bcc) β phase [3]. However, the low service temperature of Ti6Al4V (~ 300 °C) is a significant parameter that limits their potential application for high-temperature applications [4, 5]. Recently, a significant amount of research has focused on designing advanced composite materials with unique structures and desirable high-temperature properties. This has led to the development of titanium matrix composites (TMCs). TMCs are achieved by alloying the titanium matrix with hard ceramic materials such as TiB, TiC, B_4C, WC, SiC, TiB_2, TiN, and others, to elevate the properties of titanium alloys [6, 7].

Amongst the reinforcement materials, in situ synthesized TiB and TiC are considered suitable reinforcement choices due to their excellent compatibility with the titanium matrix [8, 9]. Recent literature shows that tailoring the network distribution of the reinforcement in TMCs microstructure can give promising mechanical properties including increased strength and exceptional high-temperature durability while maintaining decent tensile elongation [7, 10]. The improvement in the mechanical properties is directly related to the reinforcement material's spatial network distribution, together with their length scales. This is achieved through effective load transfer from the soft titanium matrix to hard reinforcing ceramic particulates which lead to the higher ultimate strength and creep resistance at high temperatures [10–12]. While conventional manufacturing methods have proven successful for the manufacturers of TMCs, factors such as long processing time, high tooling costs, and the need for post-processing processes remain a challenge [1, 5].

✉ Paul M. Lekoadi
PLekoadi@csir.co.za

Monnamme Tlotleng
MTlotleng@csir.co.za; Daopase@gmail.com

Charles W. Siyasiya
Charles.siyasiya@up.ac.za

Bathusile N. Masina
BMasina@csir.co.za

1 Laser Enabled Manufacturing Group, Council for Scientific and Industrial Research, Manufacturing, Photonics Centre, P.O. Box 395, Pretoria 0001, South Africa

2 Department of Mechanical Engineering Science, University of Johannesburg, Auckland Park Campus, Johannesburg 2012, South Africa

3 Department of Material Science and Metallurgical Engineering, Mineral Science Building, Universiy of Pretoria, Pretoria 0001, South Africa

As an alternative, laser metal deposition (LMD) is a type of additive manufacturing (AM) technique which uses a laser beam to form a melt pool on the surface of a metallic substrate into which metal powder is injected by a gas stream and melted to that produces three-dimensional (3D) metallic parts layer by layer [13]. Literature on the microstructural and mechanical properties of TMCs manufactured using laser-based techniques is still lacking and under development. Hence, in this study, LMD is used to manufacture TiB/Ti6Al4V-ELI composite, using Ti6Al4V-ELI and TiB_2 powders. The manufacturing of TMCs with LMD is attracting more attention from both science and engineering, with most studies focused and microstructural evolution and mechanical properties. However, the microstructure TMCs manufactured with LMD still need to be investigated. Therefore, it is important to investigate the network microstructure of TiB/Ti6Al4V manufactured with LMD to broaden the understanding, specifically for high-temperature applications. This study investigated the network microstructure and hardness properties of TiB/Ti6Al4V-ELI composite produced with the LMD using an optical microscope (OM), scanning electron microscope (SEM), and Vickers micro-hardness.

Materials and methods

Materials

A grade 23 Ti6Al4V-extra low interstitial (ELI) with particle size distribution (PSD) in the range 45–100 µm and TiB_2 powder with PSD 45–100 µm were used during deposition. The SEM images of the Ti6Al4V-ELI and TiB_2 powders are shown in Fig. 1.

The Ti6Al4V-ELI particles were spherical and smooth (Fig. 1a). In contrast, the TiB_2 particles presented irregular shape as presented in Fig. 1b. The samples were deposited on a Ti6Al4V substrate, subjected to sandblasting to prepare it for deposition.

Methods

A single-track sample of approximately 40 mm was manufactured on a LMD machine. The LMD system was coupled with an IPG fibre laser of wavelength 1073 nm and integrated with a KUKA robot and 3-way nozzles. A GTV powder system (D-57629), equipped with two powder feed hoppers, was used to deliver the powders through the carrier gas. The Ti6Al4V-ELI was deposited at a mass deposition volume of 95%, while the TiB_2 was deposited at 5%. The powder carrier gas was set at 1.5 l/min during the deposition. Argon gas was used as a protective gas, at a gas flow rate of 15 l/min to prevent the samples from oxidation. During deposition, all other process parameters were kept constant at a laser power of 1500 W, scanning speed of 0.5 m/min, and beam diameter of 2 mm.

Sample preparation and characterization

They were prepared according to metallurgical standard before they were etched with Kroll's reagent for microstructure observation. An Olympus BX51M Optical microscope and Joel JSM-6010PLUS/LA SEM were used to observe the microstructures. Hardness measurements were performed using the Matsuzawa Seiko Vickers model MHT-1 microhardness machine, applying a force of 300 gf and a dwell time of 10 s.

Results

Microstructure

Figure 2 presents the overall OM and SEM microstructures of the TiB/Ti6Al4V sample at the top, middle, and bottom, respectively.

From Fig. 2a, the deposited TiB/Ti6Al4V-ELI single-track sample did not show any obvious defects such as

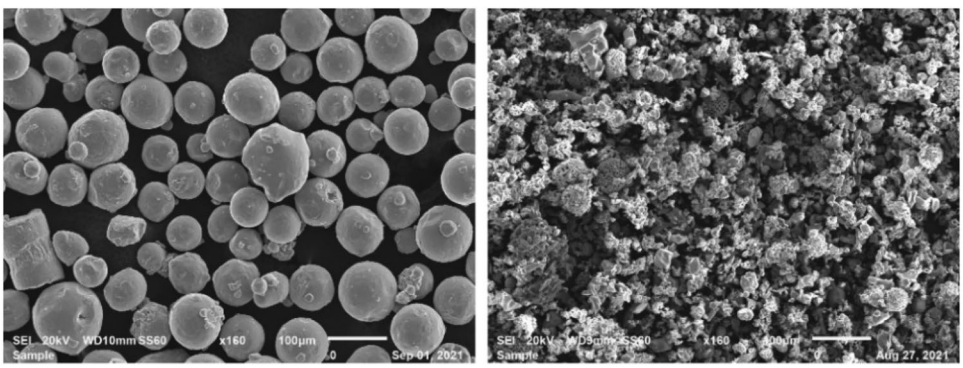

(a) (b)

Fig. 1 SEM images of the powders, **a** Ti6Al4V-ELI and **b** TiB_2

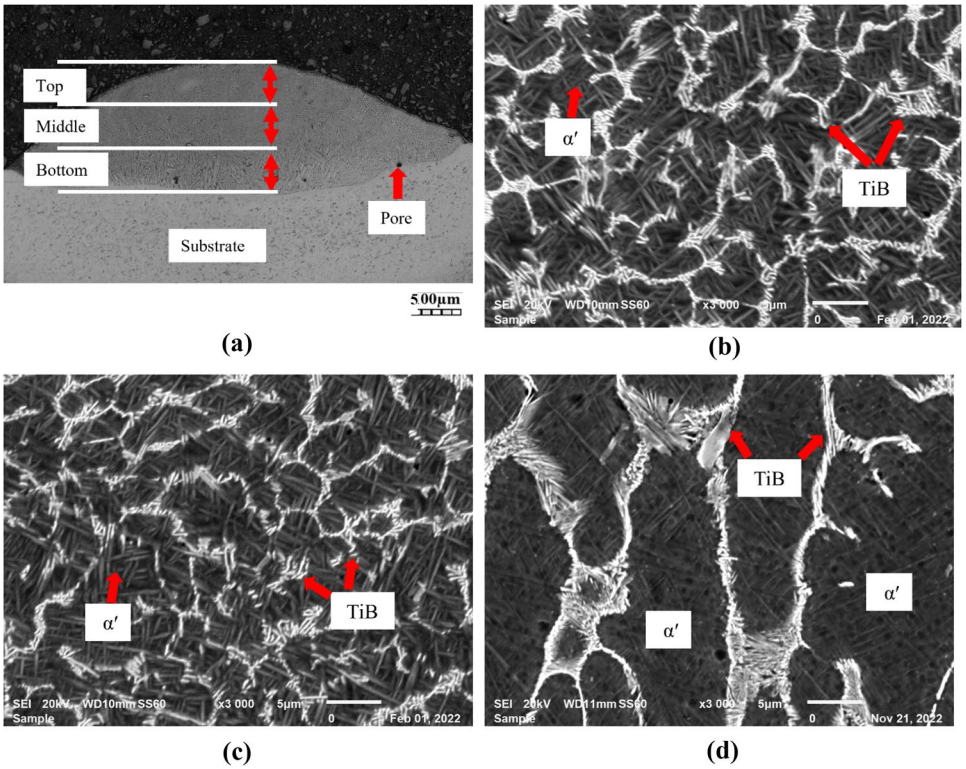

Fig. 2 Microstructures of the sample at different sections, **a** Overall single track, **b** Top, **c** Middle, and **d** Bottom

cracks, voids, or unmelted particles. However, small spherical pores were observed closer to the interface as shown in Fig. 2a. The formation of these pores was attributed to gas entrapment in the melt pool during the deposition process [7]. Furthermore, it was obvious that the sample showed different microstructural characteristics at the top and bottom sections. To study the microstructure in detail, SEM was conducted at the top, middle, and bottom, and the resulting microstructures are presented in Fig. 2b–d. As seen from Fig. 2a, the microstructure of the sample at the top section presented a matrix that composed of fully acicular martensitic α′ phase. The formation of the martensitic α′ phase was attributed to high cooling rates experienced by the sample during the LMD process which can go up to ~ 10^3–10^6 K/s [14, 15]. In fact, the martensite α′ phase transformed from β phase through a diffusionless process upon cooling of the sample [16]. According to Ahmed et al. [17], the martensite α′ phase forms within specific cooling rates in the range of 20–410 °C/s. The same type of martensitic α′ microstructure is reported in other studies on Ti6Al4V manufactured with LMD [13, 18, 19]. The martensitic microstructure is known to promote strength increase, but at the cost of ductility [19]. In such cases, the ductility can be improved by transforming the martensitic α′ phase into stable α + β phases through post-processing techniques such as heat treatment [3, 20].

Within the martensitic matrix, a quasi-continuous network structure of in situ synthesized TiB phase was evident as shown in Fig. 2c. The formation of TiB phase was attributed to the in situ reaction between the molten titanium and TiB_2 that took place during processing as defined by reaction 1 [11]:

$$Ti + TiB_2 \rightarrow 2TiB \tag{1}$$

Reaction 1 accounts for the presence of TiB on the microstructure of the sample (Fig. 2c) instead of TiB_2. Moreover, it must be noted that reaction 1 is an exothermic process, with the Gibbs free energy of formation of − 10 kcal/mol, from which the negative sign indicates a spontaneous reaction for the formation of TiB [21, 22]. Figure 2c shows that the in situ formed TiB appeared as needle-like whiskers. Similar type of TiB whiskers with needle-like morphology is reported in the literature [23, 24]. According to Ma et al. [25], when the boron (B) content in the titanium matrix is below 50 at. %, TiBw with an orthorhombic crystal structure that grows in the form of short whiskers with a needle-like morphology can be formed. Moreover, it must be noted that the network structure of the TiB whiskers is formed at the grain boundaries of the parent β phase of the titanium matrix. The formation of TiB at the β grain boundaries was due to high laser energy irradiation on the Ti6Al4V and TiB_2 powders causing primary β phase nucleation, and growth from the liquid phase during solidification and development of a steep thermal gradient between the centre edge of the molten pool surface, forming surface tension

gradient and resultant Marangoni flow [7, 26]. In contrast, Pan et al. [27] attributed the formation of quasi-continuous TiB at the grain boundaries to high cooling rates and low solubility of B in the titanium matrix. This type of microstructure was reported to enhance tensile strength and ductility at ambient temperatures [12].

Figure 2d shows that the microstructure in the middle showed similar characteristics with the top section. It was obvious from Fig. 2e that the manufactured TiB/Ti6Al4V-ELI sample showed a different grain growth morphology at the bottom section. Since this region is mostly affected by heat (heat-affected zone), larger grains of the TiB network structures were observed as can be seen in Fig. 2c, f. The increase in grain size was attributed to grain growth that was promoted by high heat input and slow cooling in this region [3]. A similar observation was made by Wang et al. [28] on Ti6Al4V alloy manufactured with LMD. According to Wang et al. [28], the grain growth at the bottom of the sample can be associated with two factors, namely, the excellent high-temperature thermodynamic stability, and direct epitaxial grain growth from the parent grains when the sample is cooling. It must be noted that the matrix remained martensitic α′ (Fig. 2e) even though there was grain growth, owing to high solidification rates.

Hardness

The hardness values of the sample at the top, middle, and bottom are represented in Table 1.

The hardness of the sample at the top section gave the highest hardness of 513 HV as presented in Table 1. The high hardness was attributed to the presence of both martensite α′ and TiB that are known to be hard [3, 11]. The hardness of the sample was slightly decreased to 503 HV from top to the middle section, owing to the similarity in microstructures of these two regions. The hardness was noticeably decreased to 483 HV at the bottom (Table 1). The decrease in hardness was attributed to the grain growth that was observed on the microstructure of the sample (Fig. 2d) [29]. According to the Hall–Petch relation, the relationship between hardness (HV) and grain size (d) can be given by Eq. 2 [29].

$$HV = HV_0 + \frac{ky}{\sqrt{d}}, \tag{2}$$

where HV_0 and ky are the material constants representing the hardness of a grain-free material and the hardening coefficient, respectively.

Table 1 Hardness value of the sample at different positions

Position	Top	Middle	Bottom
Hardness ($HV_{0.3}$)	513	504	483

Discussion

The high cooling rates during LMD influence the microstructure of TiB/Ti6Al4V-ELI composite, thereby promoting the formation of martensitic α′ matrix (Fig. 2d), that is unstable, causing strong microstructural anisotropy. The martensite α′ phase is associated with increased strength and low ductility. Furthermore, high cooling rates can also lead to high residual stress concentrations that can result in unpredicted fatigue failures and stress corrosion cracks [7, 21]. The LMD TiB/Ti6Al4V-ELI microstructure is also influenced by the formation and distribution of TiB network structure on the β-grain boundaries through an in situ reaction between titanium and TiB_2 (reaction 1). More precisely, the in situ reaction takes place at the surface of the spherical Ti6Al4V particles, resulting in the concentration of network TiB at the grain boundaries. According to Huang et al. [12], the TiB/Ti6Al4V network microstructure is equivalent to equiaxed grains, whereby TiB is formed on the β-grain boundaries. The formation mechanism of the network microstructure is demonstrated in Fig. 3.

It is clear from Fig. 3 that the TiB whiskers are preferably formed on the boundaries of the β-Ti due to high surface tension created by a steep thermal gradient between the edges of the molten pool [20]. TiB/Ti6Al4V with a network architecture is known to be beneficial for high-temperature mechanical properties and enhanced oxidation resistance thereby prohibiting grain boundary softening [12]. Using sintering methods, Huang et al. reported that a TiB/Ti6Al4V with a network microstructure improved strength up to 600 °C. The strengthening effect was attributed to the strong network boundary between the matrix and reinforcement enabled by the needle-like TiB whiskers. A similar microstructure with network distribution of TiB was manufactured by laser-engineered net shaping (LENS) [26].

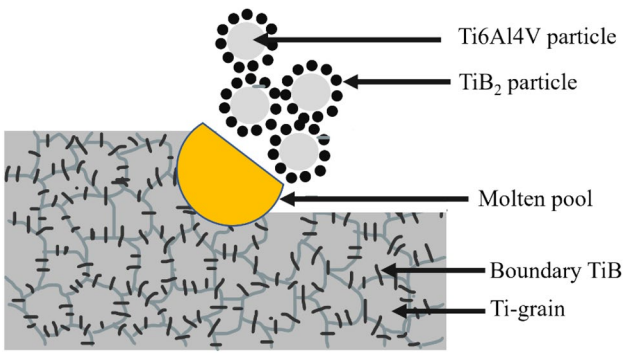

Fig. 3 Schematic illustration for the formation of network microstructure

Conclusion

In this paper, an optimized single-track TiB/Ti6Al4V-ELI composite sample containing 5% vol TiB_2 was manufactured using laser metal deposition to understand the novel network microstructural characteristics and hardness properties for their use in high-temperature applications. The overall matrix of the composite was fully martensitic α′ with a quasi-continuous network of in situ synthesized TiB whiskers forming on the titanium grain boundaries. Two different grain growth morphologies were observed at the top and bottom of the sample, with bigger grains forming at the bottom closer to the substrate due to slow cooling rate in these regions. The increase in grain size at the bottom of the sample led to a noticeable decrease in hardness to 483 HV; Hall–Petch relationship. To the best of our knowledge, there is a novelty in this work in that a novel network microstructure has been achieved for the first time using LMD technique as opposed to conventional manufacturing methods as widely reported.

Acknowledgments The authors would like to thank the Council for Scientific and Industrial Research (CSIR) for offering laboratory resources. The Department of Science and Innovation is thanked for funding the work through the Collaboration Program in Additive Manufacturing (CPAM), grant number HLM4BMX. Mr. Samuel Skhosane is thanked for his assistance with the experimental work.

Funding Open access funding provided by Council for Scientific and Industrial Research.

Data availability The dataset generated and analysed during the current study are available from the corresponding author on reasonable request.

Declarations

Conflict of interest On behalf of all authors, the corresponding author states that there is no conflict of interest.

References

1. Z.G. Zhou, Y.Z. Liu, Z.H. Liu, Q.K. Zhan, K.D. Wang, Composite B **207**, 1–10 (2021)
2. L. Zhao, C. Cui, S. Liu, L. Zhao, N. Li, Mater. Sci. Eng. A **663**, 8–16 (2016)
3. P. Lekoadi, M. Tlotleng, K. Annan, N. Maledi, B. Masina, Metals **255**, 1–15 (2021)
4. I. Inagaki, Y. Shirai, T. Takechi, N. Ariyasu, Nippon Steel Tech. Rep **106**, 22–27 (2014)
5. H. Attar, M. Bonisch, M. Calin, L.C. Zhang, S. Scudino, J. Eckert, Acta Mater. **76**, 13–22 (2014)
6. W. Zhou, X. Sun, K. Kikuchi, N. Nomura, K. Yoshimi, A. Kawasaki, Mater. Des. **137**, 276–285 (2018)
7. C. Cai, S. He, L. Li, Composites **164**, 546–558 (2019)
8. S. Li, Y. Han, H. Zhou, G. Huang, J. Le, X. Wang, W. Lu, Mater. Sci. Eng. A **829**, 1–12 (2022)
9. L. Sousa, A.C. Alves, N.A. Costa, J. Alloys Compd. **896**, 1–9 (2022)
10. A.A. Da Silva, J.F. Dos Santos, T.R. Strohaecker, Compos. Sci. Technol. **65**, 1746–1755 (2005)
11. L.J. Huang, L. Geng, H.Y. Xue, Mater. Sci. Eng. A **528**, 2859–2862 (2011)
12. L. Huang, Q. An, L. Geng, Adv. Mater. **33**, 1–27 (2021)
13. C. Zhong, J. Liu, T. Zhao, T. Schopphoven, J. Fu, A. Gasser, J.H. Scheifenbaum, Appl. Sci. **764**, 1–12 (2020)
14. T. DebRoy, H.L. Wei, J.S. Zuback, T. Mukherjee, J.W. Elmer, J.O. Milewski, A.M. Beese, A. Wilson-Heid, A. De, W. Zhang, Prog. Mater. Sci. **92**, 112–224 (2018)
15. A. Azarniya, X.G. Colera, M.J. Mirzaali, S. Sovizi, F. Bartolomeu, M.K. Weglowski, J. Alloys Compd. **808**, 163–191 (2019)
16. D. Liu, S.Q. Zhang, A. Li, H.M. Wang, J. Alloys Compd. **496**, 189–195 (2010)
17. T. Ahmed, H.J. Rack, Mater. Sci. Eng. A **243**, 206–211 (1998)
18. Y. Fu, N. Guo, G. Wang, M. Yu, Q. Cheng, D. Zhang, Mater. Des. **197**, 1–13 (2021)
19. S.A. Shalnova, M.O. Gushchina, D.A. Strekalovskaya, E.L. Alekseeva, O.G. Klimova-Korsmik, J. Alloys Compd. **899**, 1–8 (2022)
20. E. Dolgun, E. Zemlyakov, S. Shalnova, M. Gushchina, V. Promahov, Mater. Today Commun. **30**, 688–693 (2020)
21. Q. Zhang, W. Sun, S. Xu, X. Zhang, J. Wang, C. Si, J. Alloys Compd. **922**, 1–12 (2022)
22. P.K. Verma, S. Warghane, U. Nichul, Mater. Charact. **172**, 1–11 (2021)
23. H. Li, Z. Yang, D. Cai, Mater. Des. **185**, 1–11 (2020)
24. E. Fereiduni, A. Ghasemi, M. Elbestawi, Add. Manuf. **50**, 1–19 (2022)
25. F.C. Ma, P. Liu, W. Li, X.K. Liu, X.H. Chen, K. Zhang, D. Pan, W.J. Lu, Sci. Rep. **6**, 1–9 (2016)
26. Y. Hu, W. Cong, X. Wang, Y. Li, F. Ning, H. Wang, Composites **133**, 91–100 (2018)
27. D. Pan, X. Zhang, X. Hou, Mater. Sci. Eng. A **799**, 1–6 (2021)
28. J. Wang, L. Li, P. Lin, J. Wang, Opt. and Laser Technol. **105**, 195–206 (2018)
29. J.S. Zuback, T. Debroy, Mater. **11**, 2–41 (2018)